# One-Way Fluxes of $\alpha$-Aminoisobutyric Acid in Ehrlich Ascites Tumor Cells

## *Trans Effects and Effects of Sodium and Potassium*

JOHN A. JACQUEZ

From the Department of Physiology, University of Michigan, Ann Arbor, Michigan 48104

A STRACT One-way fluxes in the steady state and one-way influxes at zero intracellular concentrations were measured for $\alpha$-aminoisobutyric acid (AIB) in Ehrlich ascites tumor cells at 32°C. The one-way fluxes show *trans* effects in the concentration of AIB and are dependent on sodium levels. The one-way fluxes for initial influx and for the steady state were fitted with the equations derived for the frequently used two-state carrier model. Estimates of the parameters of these equations were obtained with use of nonlinear least squares. These gave relatively good fits of the flux data and the data on steady-state distribution ratios. The two-state carrier model predicted a *trans* inhibition of one-way influx and a *trans* stimulation of one-way efflux. The former phenomenon has been demonstrated for AIB transport in Ehrlich ascites cells and there is evidence, though less firm, for the latter.

### INTRODUCTION

The initial influx of an amino acid into Ehrlich ascites tumor cells is well described by Eq. 1 which is a sum of a Michaelis-Menten term and a linear term in the extracellular concentration, $c_e$.

$$J_{in} = \frac{J_{M_{in}} c_e}{K_{m_{in}} + c_e} + k c_e. \quad (1)$$

A similar expression in the intracellular concentration describes initial effluxes quite well, Eq. 2.

$$J_{ef} = \frac{J_{M_{ef}} c_i}{K_{m_{ef}} + c_i} + k c_i. \quad (2)$$

Many of the early pump-leak models of net transport used combinations of the terms in Eqs. 1 and 2 (1–4). However, there is now considerable evidence to

show that the one-way fluxes depend on the *trans* concentrations, i.e., the concentration on the side towards which the flux is directed, as well as on the *cis* concentrations. This evidence consists of *trans* stimulation of uptake (1, 5–13) as well as of *trans* inhibition (8, 14–17). In the latter, the initial influx of an amino acid is decreased by first loading the cell with the same or another amino acid. In *trans* stimulation it is increased. However, there is also evidence that *trans* stimulation for some of the neutral amino acids is an exchange mediated by a system distinct from the active transport system (9, 10, 18). The existence of *trans* effects shows that Eqs. 1 and 2 must be wrong in general and that the equations for one-way fluxes must depend on the *trans* as well as the *cis* concentrations.

Interestingly most of the carrier models that have been postulated over the last two decades predict *trans* effects. Thus, although current theories predict *trans* effects and there is more than sufficient evidence for *trans* effects, experimental studies of kinetics have been for the most part restricted to conditions under which Eqs. 1 and 2 have been adequate for the interpretation of the experimental data. The basic carrier model and notation that I will use are shown in Fig. 1. This is a two-state carrier model, i.e., the carrier and the carrier substrate complex can each occupy one of two positional states, the transitions between the states being given in terms of the rate constants in Fig. 1. The equations for the one-way fluxes, with and without assuming equilibrium for the binding reactions at each surface, have been derived for this model and a number of related models (19–26). With the development of the evidence for cotransport of sodium with the neutral amino acids, reviewed in

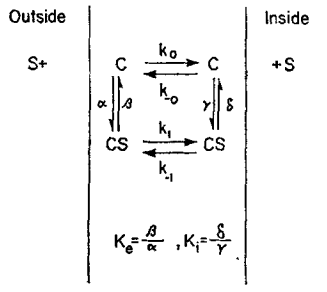


FIGURE 1

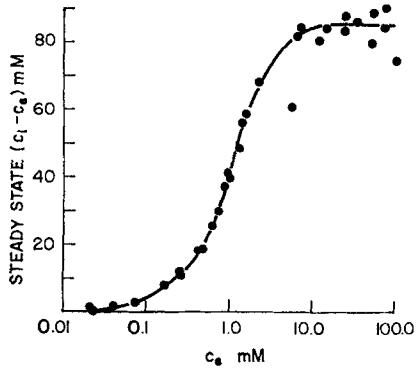


FIGURE 2

FIGURE 1. Two-state carrier model. The constants $\alpha$, $\beta$, $\gamma$, $\delta$ are rate constants for the binding reactions, whereas $k_o$, $k_{-o}$, $k_1$, $k_{-1}$ are transition rate constants for the transitions between the two states, one at each side of the membrane.

FIGURE 2. Concentration difference, $c_i - c_e$, attained in steady state as function of extracellular concentration of AIB. Ehrlich ascites tumor cells in high sodium Krebs-Ringer phosphate.

references 27 and 28, new carrier models that included binding of sodium as well as of substrate had to be formulated. The rate equations for a number of ion cotransport models have been derived and are available in the literature (29–35), including a model for glycine transport in pigeon erythrocytes in which there is a cotransport of two sodiums with each glycine (36, 37). Although these models of ion cotransport differ in their assumptions about how many different ions can be involved in the reaction sequences and most do not include the effect of the membrane potential, all assume equilibrium for the binding reactions at each surface.

The carrier model shown in Fig. 1, with the assumption of equilibrium for the binding reactions at each surface gives Eqs. 3 and 4 for the unidirectional fluxes if one substrate is present.

$$J_{\text{in}} = \frac{A_o c_e + A_2 c_e c_i}{1 + B_o c_e + B_1 c_i + B_2 c_e c_i} + k c_e. \tag{3}$$

$$J_{\text{ef}} = \frac{A_1 c_i + A_2 c_e c_i}{1 + B_o c_e + B_1 c_i + B_2 c_e c_i} + k c_i. \tag{4}$$

In terms of the rate constants in Fig. 1, the parameters in 3 and 4 are as follows:

$$A_o = \frac{C_o k_{-o} k_1}{K_e(k_o + k_{-o})}, \qquad B_o = \frac{(k_{-o} + k_1)}{K_e(k_o + k_{-o})}; \tag{5}$$

$$A_1 = \frac{C_o k_o k_{-1}}{K_i(k_o + k_{-o})}, \qquad B_1 = \frac{(k_o + k_{-1})}{K_i(K_o + k_{-o})}; \tag{6}$$

$$A_2 = \frac{C_o k_1 k_{-1}}{K_e K_i(k_o + k_{-o})}, \qquad B_2 = \frac{(k_1 + k_{-1})}{K_e K_i(k_o + k_{-o})}; \tag{7}$$

where, $K_e = \beta/\alpha$, $K_i = \delta/\gamma$, $C_o$ = total carrier concentration. From relations 5–7 it can be shown that the constants $A_o$, $A_1$, $A_2$, $B_o$, $B_1$, $B_2$ are constrained by relation 8,

$$\frac{B_2}{A_2} = \frac{B_o}{A_o} + \frac{B_1}{A_1} - \frac{A_2}{A_o A_1}. \tag{8}$$

If ion cotransport is involved the parameters $A_o$, $A_1$, $A_2$, $B_o$, $B_1$, $B_2$ are functions of rate constants, ion concentrations, and the membrane potential but constraint 8 still holds. The expressions for the parameters for a sodium cotransport model are given in the Appendix. Note that the *trans* concentrations appear in each of Eqs. 3 and 4 for unidirectional fluxes. If in experiments on the kinetics of uptake, one looks only at initial influxes and effluxes, the transport terms in 3 and 4 reduce to Michaelis-Menten form and it is possible to estimate only $A_o$, $B_o$, $A_1$, and $B_1$ which are simply related to the $K_m$'s and the maximal fluxes, as follows:

$$J_{M_{\text{in}}} = A_o/B_o, \qquad K_{m_{\text{in}}} = 1/B_o, \qquad J_{M_{\text{ef}}} = A_1/B_1, \qquad K_{m_{\text{ef}}} = 1/B_1.$$

If one examines only initial fluxes, there is no way of estimating $A_2$ and $B_2$. In fact, little has been done to test whether Eqs. 3 and 4 describe the one-way fluxes for a wide range of conditions.

The present study grew out of an investigation of the sodium dependence of the one-way fluxes of $\alpha$-aminoisobutyric acid (AIB) in the steady state in Ehrlich ascites cells. I found that the dependence of the one-way eflux of AIB on intracellular concentration was clearly non-Michaelis-Menten in form. This observation was the initial stimulus for the work reported here in which one-way influxes and effluxes have been measured in the steady state and the influx has been measured for $[AIB]_i = 0$. Strong *trans* effects are demonstrated in the one-way fluxes and rough estimates of all of the parameters in Eqs. 3 and 4 have been obtained for one set of values of the extracellular concentrations of sodium and potassium.

## METHODS AND MATERIALS

The properties of our line of Ehrlich ascites and the general procedures used in this laboratory have been described (18). The cells used in these experiments were all from our Lo line and were harvested at 6–8 days after inoculation of the animals. The incubations in all experiments were at 32°C. This was chosen for the steady-state experiments to slow down the equilibration of tracer at the low concentrations of AIB and was then used for all experiments. AIB was chosen for this study because it appears to be transported almost entirely by the A system (29).

### *Steady-State Experiments*

After harvesting the cells, they were washed once with a Krebs-Ringer phosphate which was made up to contain the following millimolar concentrations of ions: $Na^+$ = 150, $K^+$ = 7.6, $Cl^-$ = 135, $Ca^{++}$ = 0.45, $Mg^{++}$ = 0.63, $SO_4^{=}$ = 0.63, and 12.9 of mono- and dibasic phosphate. The pH values fell in the range 7.35–7.40. The AIB solutions were made up in Krebs-Ringer phosphate without adjustment of the osmolarity so as to maintain the same ion concentrations extracellularly for all AIB concentrations. The cells were resuspended in AIB twice the concentration chosen for the experiment and were incubated for 10 or 20 min at 32°C; the 10-min incubation was used for the concentrations below 2 mM, the 20 min for higher concentrations. The suspension was chilled, centrifuged, and resuspended in AIB at the concentration chosen for the experiment and incubated again for 10 or 20 min, 10 min for concentrations below 2 mM, 20 min for higher concentrations. This was repeated once more but the incubation times were extended to 20 and 30 min and then the tracer equilibration was started. The initial two incubations and washes with AIB were designed to wash out intracellular amino acids that exchanged readily with AIB so as to reduce their effect in the final equilibration with [$^{14}$C]AIB.

The above-mentioned procedures were carried out simultaneously on two batches of suspension which differed only in that tracer [$^{14}$C]AIB was present from the start in one, flask I, whereas no tracer was present in the other, flask II. Flask I was used to measure uptake and to check that a steady state had been obtained. The volume of

each batch was 50 ml and incubations were carried out in 1,000-ml Erlenmeyer flasks in a shaker bath. The suspensions were shaken at about 90 oscillations per minute. Packed cell volumes fell in the range 5–10%. At the end of the third incubation a tracer amount of [$^{14}$C]AIB was injected into flask II and the incubation was continued. Samples were taken at various times from I and II by pipetting 2 ml into 12 ml of cold Krebs-Ringer phosphate or, in the later experiments, into 12 ml of a choline Ringer phosphate. Ostwald-Folin pipettes were used and the sample was allowed to drain by gravity into the cold salt solution and the pipette was blown out; the time of the sample was taken as the time at which one-half of the pipette had drained and was measured with a stopwatch. The samples were centrifuged in a cold room and the pellet and supernatant fluid were separated for analysis for $Na^+$ and $K^+$ and for counting for [$^{14}$C]. Another 2-ml sample was pipetted into chilled tared tubes which were centrifuged in the cold, were drained, and were then used to obtain wet and dry weights. The extracellular space in the packed pellets was determined in parallel experiments with use of [$^{14}$C]sorbitol. The maximum difference in intracellular concentrations in flask I found over the period of tracer equilibration in flask II was 10% and in most experiments it was less than 5% so the conditions were always close to steady state during the tracer equilibration.

Some characteristics of the steady-state concentration process for AIB under these conditions are shown in Figs. 2–5. As may be seen in Fig. 2 there is a maximum concentration difference in AIB which these cells can maintain and this is attained at a $c_e$ of 6–10 mM; from 6 mM up to 100 mM extracellular AIB these cells maintain an almost constant concentration difference of about 85 mM across the cell membrane. The cells take in water as intracellular AIB increases. Fig. 3 gives the pellet water per gram dry weight in the steady state for different extracellular concentrations of AIB. The maximum swelling occurs for extracellular concentrations of 6–10 mM, the values for which the maximum concentration difference is first attained. However, the pellet water per gram dry weight is only about 13% greater at the maximum than at the mean value for low extracellular concentrations. Let $V_o$ be the cell water for the cells

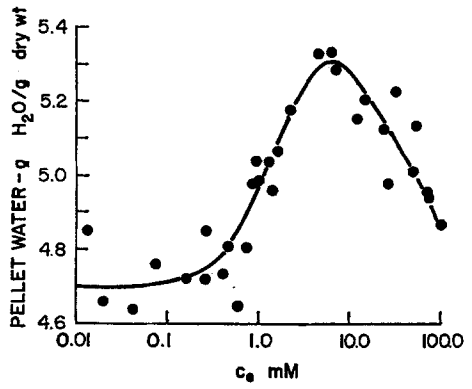


FIGURE 3. Swelling of Ehrlich ascites cells for steady-state accumulation of AIB. Pellet water per gram dry weight as function of extracellular concentration of AIB. The AIB was added to Krebs-Ringer phosphate, so osmolality was not adjusted.

in Krebs-Ringer solution and $V$ be the cell water in the steady state for AIB concentration difference of $c_i - c_e$ and let $x$ be the osmolality of the Krebs-Ringer phosphate, approximately 300 mosmol. Then if one assumes that the ascites tumor cells act as ideal osmometers, $\sigma_{AIB} = 1$, and that the osmotically active material of the cell, other than AIB, is diluted by entering water but that none is added or lost then it is easy to show that Eq. 9 should hold. Fig. 4 gives a plot of the reciprocal of the pellet water against $c_i - c_e$.

$$\frac{1}{V} = \frac{1}{V_o} - \frac{c_i - c_e}{xV_o}. \tag{9}$$

The slope is much smaller in absolute value than the slope predicted by this simple theory suggesting that not all of its assumptions apply to these cells. There is evidence

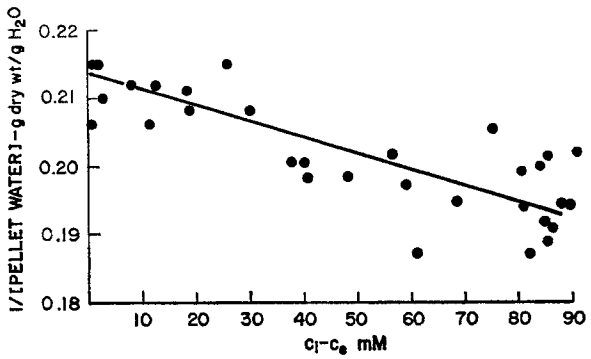


FIGURE 4. Plot of inverse of pellet water per gram dry weight against the concentration difference, $c_i - c_e$, of AIB.

of loss of osmotically active material. As shown in Fig. 5 intracellular potassium concentration decreases considerably, much more than the dilution expected from increase in cell water. There is actually a small increase in intracellular sodium at high AIB concentrations but it was only in the range of 5–10 mM, not nearly enough to make up for the decrease in potassium. The decrease in potassium is a well-known finding first described by Riggs et al. (38). The peak in the swelling shown in Fig. 3 is understandable in light of the results in Figs. 2 and 5. The osmotic effect of AIB increases until $c_i - c_e$ becomes constant, at $c_e$ = 6–10 mM. However, the decrease in intracellular potassium as $c_i$ increases suggests that the cells continued to lose osmotically active materials with increase in steady state $c_i$. Hence, there must be a peak in osmotic effect when these two opposing trends balance out.

The pH values after incubation fell in the range 7.20–7.39 in 31 experiments and had a mean value of 7.30 with a standard deviation of 0.047. Measured extracellular sodium varied from 135 to 147.6 meq/liter and had a mean of 143 meq/liter. Extracellular potassium varied between the limits 8.1–10.1 meq/liter and had a mean of 8.8 meq/liter. Intracellular sodium and potassium were more variable. Intracellular sodium had a mean of 20 meq/kg $H_2O$ and varied from 15 to 25. Intracellular potassium had a mean of 154 meq/kg $H_2O$ but varied systematically as shown in Fig. 5

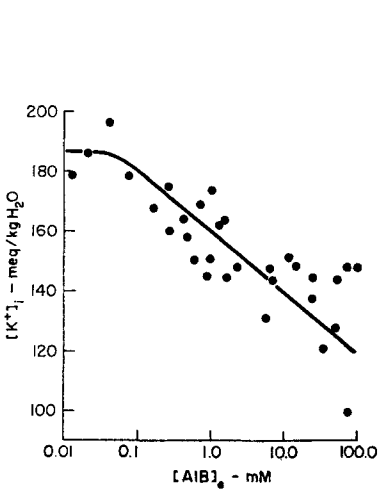


FIGURE 5

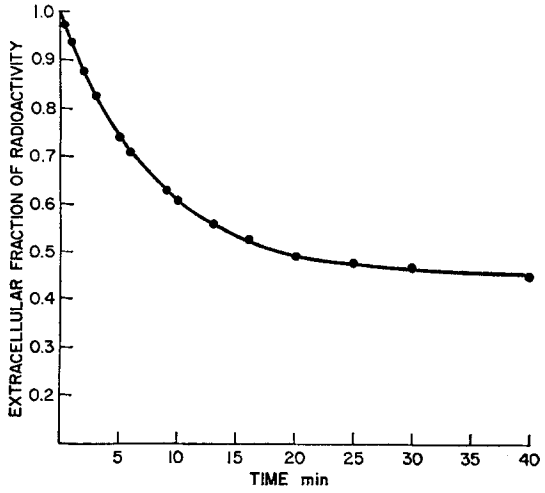


FIGURE 6

FIGURE 5. Dependence of intracellular potassium on extracellular AIB in the steady state.

FIGURE 6. Steady-state equilibration of [$^{14}$C]AIB. A tracer amount of [$^{14}$C]AIB was added at $t = 0$ to cells that had accumulated cold AIB to a steady-state level of $c_i = 58.0$ mM for $c_e = 1.55$ mM. Extracellular and intracellular radioactivity were followed. The fraction extracellular is about 0.45 at the plateau.

Another set of 49 steady-state experiments was run in which extracellular sodium and potassium were varied. Choline replaced sodium in these experiments. The pH values fell in the same range as for the previously mentioned set and had a mean value of 7.298.

*Analysis of Steady-State Experiments*

To within the accuracy of the experiments the intracellular AIB equilibrated as a single compartment. Thus no more than a few percent of the intracellular AIB can be in another pool. This agrees with the findings of Heinz (39) on glycine equilibration in Ehrlich ascites and of Kipnis et al. (40) on equilibration of leucine in rabbit lymph node cells, glycine in guinea pig lymph node cells, and proline in rat diaphragm. Fig. 6 shows the time-course of change in relative radioactivity in the extracellular phase from an experiment in which $c_e$ was 1.55 mM and $c_i$ was 58.0 mM. If the intracellular AIB behaves as a single compartment then the relative radioactivity extracellularly is given by Eq. 10 (p. 122 of reference 41).

$$\frac{\epsilon_1(t)}{\epsilon_1(t) + \epsilon_2(t)} = \frac{f_{21}}{f_{12} + f_{21}} e^{-(f_{12}+f_{21})t} + \frac{f_{12}}{f_{12} + f_{21}}. \qquad (10)$$

Here $\epsilon_1(t)$ is the extracellular radioactivity and $\epsilon_2(t)$ is intracellular radioactivity, $f_{12}$ is the fraction of intracellular AIB leaving the cells per unit time, and $f_{21}$ is the fraction of extracellular AIB entering the cells per unit time. If the plateau value is subtracted from $\epsilon_1/(\epsilon_1 + \epsilon_2)$ one should obtain a straight line on a semilogarithmic plot. This is

shown in Fig. 7. The same curve can be obtained from a plot of the fraction of radioactivity in intracellular phase. Because the plateau in Fig. 6 had to be estimated a number of values near the estimated plateau value were tried and by trial and error, the one found that gave the best straight line. The value that gave the best linear plot was always within a few percent of the plateau value estimated from the graph. From theory, the plateau value should also be $q_1/(q_1 + q_2)$, the fraction of total AIB extracellular, and this was also always within a few percent of the value that gave the best linear plot. From the slope of the semilogarithmic plot one obtains the one-way flux $\rho = q_1q_2[f_{12} + f_{21}]/[q_1 + q_2]$, for the sample. This was divided by the dry weight to

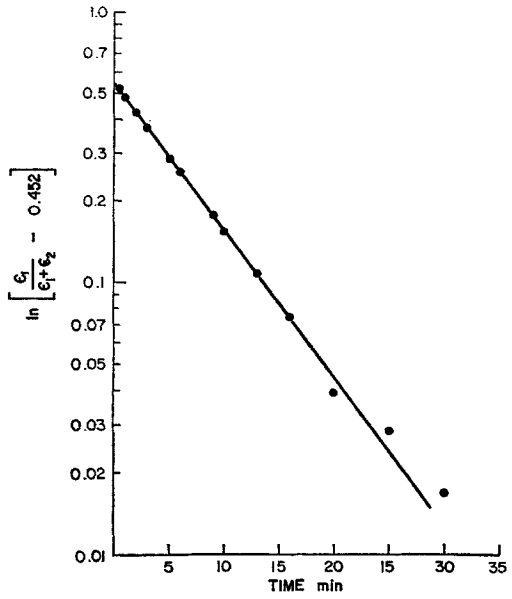


FIGURE 7. Semilogarithmic plot of deviation from plateau value of extracellular fraction of radioactivity for data in Fig. 6.

give total one-way flux in millimoles per gram dry weight per minute. This then is the unidirectional flux into and out of the cells.

*Experiments on Initial Influxes*

Another group of experiments was set up to estimate initial one-way influx for $c_i = 0$. In these experiments the cells also underwent two preliminary incubations at 32°C for 10 min each but in the Krebs-Ringer phosphate without any added amino acid. My intention was to treat these cells in the same way as the cells in the steady-state experiments had been treated. However, because AIB was not present during the preliminary incubations, it is unlikely that the levels of endogenous amino acids that readily exchange with AIB could have been decreased to levels as low as in the steady-state experiments. This raises the question of the comparability of the data from the two types of experiments. Recently Christensen et al. (42) have reported the levels of

endogenous amino acids in Ehrlich ascites tumor cells after four 5-min incubations in Krebs-Ringer bicarbonate or two incubations in the Krebs-Ringer solution followed by two in 10 mM AIB or 0.1 mM AIB. In the former the total endogenous pool was not quite halved, in the latter it fell to less than one-third its original level for the incubation in 10 mM AIB and not quite so much for the incubation in 0.1 mM AIB. One of the reviewers of the first draft of this paper suggested that the sum of endogenous alanine, serine, and threonine be taken as an estimate of AIB exchangeable amino acids and that the effect of a comparable level of intracellular AIB on one-way influx be estimated. The sum, ala + ser + thr, was about 1 mM for the AIB incubated cells so I will use 2 mM as the estimate for the cells incubated in Krebs-Ringer phosphate. Using the parameters for Eq. 3 obtained from uncorrected data, line 5 in Table I, one can calculate that for an extracellular AIB of 0.1 mM the one-way influx for $c_i = 2$ mM is only 10% less than for $c_i = 0$ and that the effect is smaller than this for $c_o > 0.1$ mM. Such a small correction in the data on one-way influx would have little effect on the parameters estimated for Eqs. 3 and 4. Because of the smallness of the estimated correction and its uncertainty the raw data on one-way influx were not corrected.

After the first two incubations and washes the cells were resuspended in KRP at twice final cell concentrations. The incubation vessels were 125-ml Erlenmeyers with sidearms. Five milliliters of cell suspension were pipetted into the main part of a flask and 5 ml of a solution of AIB were pipetted into the sidearm. The vessels were incubated, with shaking, for 10–30 min before tipping and mixing. The long incubation before tipping was used to allow the cells time to recover from the period in the cold, during which there is a rapid entry of sodium into the cells (43). After incubation, these cells had average intracellular sodiums and potassiums of 23.4 and 167 meq/kg $H_2O$, respectively, so they were comparable with the cells of the steady-state experiments in electrolyte composition. The average pH value after incubation was 7.34 in these experiments. Samples were taken at 0.5, 1.0, 1.5, and 2.0 min by pipetting 2 ml of suspension into cold choline Ringers and centrifuging in the cold to separate the pellet of cells from the supernatant fluid. As for the steady-state experiments the extracellular space was calculated from parallel measurements on the [$^{14}$C]sorbitol space. The net flux was calculated for each sample time and the four values were fitted with a quadratic, $J = a_o + a_1 t + a_2 t^2$, by least squares. The constant, $a_o$, is the estimated flux at $t = 0$. The standard error of the estimate of $a_o$ was on the average 3% of the value of $a_o$ and varied from 0.1% up to 11%. The calculated zero time flux, $a_o$, was 15–50% larger than the 1-min flux calculated directly from the uptake at 1 min. To estimate the error in incubation time due to mixing and the method of pipetting, the amount of AIB per unit dry weight in the cells was also fitted with a quadratic by least squares, $q = b_o + b_1 t + b_2 t^2$. The constant $b_o$ was close to zero but in almost all cases it had a small positive value. The time needed to accumulate $b_o$ at the initial flux $a_o$, $t^* = b_o/a_o$ was taken as an estimate of the bias in the incubation times. The average value of $t^*$ was $-0.07$ min with a standard deviation of 0.05 min; the extreme values were $-0.17$ and $+0.17$. There were three positive values out of the 36. This error in timing would have given only a few percent error in calculated fluxes. No attempt was made to recalculate the data with this correction for timing included because it was so small.

*Experiments on Efflux*

A number of experiments on efflux were carried out in the hope they would provide data on efflux as good as those obtained in the experiments on influx. After a preliminary incubation for 10 min at 32°C the cells were chilled, centrifuged, and resuspended in [$^{14}$C]AIB and were incubated for 10–20 min, washed, resuspended in fresh AIB, and incubated for 20 min. The cells were then washed twice with cold KRP to give a packed cell volume of 0.15–0.29. Two milliliters of this suspension were put in the sidearm of an incubation vessel and 12 ml of KRP or 23 mM unlabeled AIB warmed to 32°C, were placed in the main well. After an incubation of 2 min the vessel was tipped and the contents mixed. Samples were taken at 0.5, 1.0, 1.5, and 2.0 min. It was found that the initial extracellular concentration of labeled AIB due to leakage and incomplete washing was in the range $\frac{1}{200}$–$\frac{1}{300}$ of the intracellular concentration. The intracellular AIB per unit dry weight was fitted with the quadratic, $q = b_o + b_1 t + b_2 t^2$, by least squares. From $b_o$ the initial intracellular concentration was calculated; $b_1$ was the estimated efflux at $t = 0$. Thus in the experiments in which efflux into KRP was measured, $b_1$ was the net efflux for the initial $c_i$ and for $c_e$ equal approximately to $c_i/250$. For the experiments in which efflux was into 20.5 mM unlabeled AIB, the labeled material was so diluted by the cold AIB that $b_1$ may be considered to be the one-way efflux for $c_e \simeq 20$ mM.

The one-way effluxes turned out to be unreliable whether they were calculated from the decrease in intracellular AIB or from the rate of accumulation of extracellular AIB. In over one-half of the runs the standard error of $b_1$ was greater than 20 % of $b_1$. Furthermore, because of the brief warm-up period that was used to prevent excessive leakage from the cells these cells had not fully recovered their ion gradients and were not truly comparable with those used for the steady state and the initial influx studies. The results were so poor, almost none were used. The methods are given to document this problem and because the effluxes into cold 20 mM AIB were used to obtain a rough estimate of $A_2$ that was used as an initial guess of the value of $A_2$ in a nonlinear least squares estimation of the parameters of Eqs. 3 and 4. The efflux data were not used in the parameter estimation.

## RESULTS

*Steady-State Studies for $[Na^+]_e = 143$, $[K^+]_e = 8.8$*

Major emphasis in this work was put on studies at the steady state for a number of reasons. Most important is the fact of the steady state, in ions, water, and in AIB. In initial flux studies there is an accompanying net influx of water and of sodium. Thus, there is the possibility of interaction of AIB flux with the net water flow as well as that of a change in membrane potential during the uptake. There is also the possibility of a contribution to the net flux of AIB due to exchange with intracellular amino acid pools. All of these effects are either avoided or minimized in studies in steady states.

Fig. 8 shows the steady-state unidirectional flux as a function of extracellular (—●—) and intracellular (—○—) concentration. For each of these curves

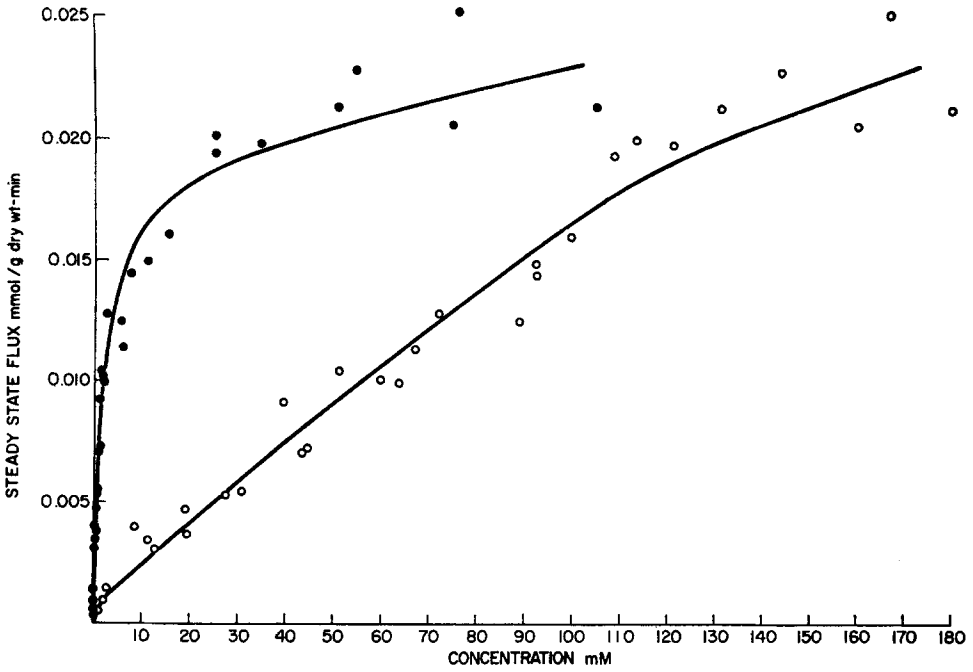


FIGURE 8. One-way flux in the steady state as function of the extracellular concentration (—●—) and of the intracellular concentration (—○—). The curves are the calculated values given by Eqs. 3 and 4 for $k = 0.056$, $A_o = 23.5$, $B_o = 577$, $A_1 = 0.322$, $B_1 = 77$, $A_2 = 440$, $B_2 = 28{,}715$.

each point comes from one experiment, so corresponding to the flux measured in each experiment there is a point on each of the two curves. The flux vs. $c_e$ curve might be interpreted as having a saturable component that is Michaelis-Menten in form but this is certainly not true for the flux vs. $c_i$ curve. The continuous curves were calculated from Eqs. 3 and 4 with the parameter set that gave the best simultaneous fit of the initial flux and the steady-state data. Along with the many advantages of steady-state studies there are also some possible drawbacks that should be kept in mind when interpreting these results. As was pointed out in the Methods section the swelling is small and in and of itself is probably of small consequence. Over the range of AIB concentrations covered there is a change in osmolality and in intracellular potassium concentration. The osmolality at the low concentrations in Fig. 8 is about 300 mosmol whereas at the very top concentrations, it is 400 mosmol, an increase of one-third. However, over a major portion of the curves shown in Fig. 8, for $c_e < 30$ mM and $c_i < 120$ mM, there is less than a 10% change in osmolality so it seems unlikely that this change can have much effect on the transport system. The concomitant decrease in intracellular potassium is of a larger magnitude, as may be seen in Fig. 5, and suggests that as the AIB concentra-

tion increases there is a gradual shift in the steady state in the cellular ions. The decrease in $[K^+]_i$ may also be accompanied by a decrease in the steady-state membrane potential as intracellular AIB increases. Thus, although the data in Fig. 8 are certainly steady-state fluxes, the nature of the steady states may change as the AIB concentration increases. In this sense the curves in Fig. 8 might be thought of as passing through a series of adjacent steady states for which the transport parameters may differ somewhat. Therefore, the parameters of Eqs. 3 and 4 obtained by fitting these data may represent an average over a set of adjacent steady states of the cells. Fig. 9 shows the steady-state concentration ratio, $c_i/c_e$, as function of $c_e$. The continuous curve is the distribution ratio at steady state predicted from the parameter set that gave the best simultaneous fit of the initial flux and steady-state data.

*Initial Influx*

The initial one-way influxes for $c_i = 0$ calculated from the initial flux data in five experiments are given in Fig. 10. The different experiments are indicated by the different symbols. Note how much this differs from the one-way influx at the steady state in Fig. 8. The maximum value obtained for the latter was 0.025 mmol/(g dry wt-min) whereas the $J_{M_{in}}$ for one-way influx at $c_i = 0$ was 0.04. The continuous curve in Fig. 10 was calculated from Eq. 3 for the parameters obtained by simultaneous fitting of the initial flux data and the steady-state flux data. The parameter fitting is discussed below. An inverse plot of 19 of the data points of Fig. 10 is shown in Fig. 11. The points at the three lowest and five highest concentrations were not used; the former because of the high error in the inverses for small fluxes and concentrations, the latter

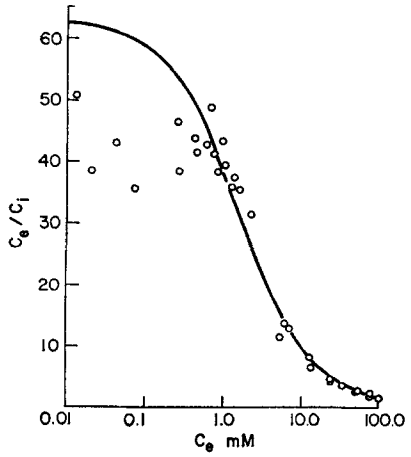


FIGURE 9. Concentration ratio in the steady state as function of extracellular concentration. The curve is calculated from Eqs. 3 and 4 with use of the values of the parameters given for Fig. 8.

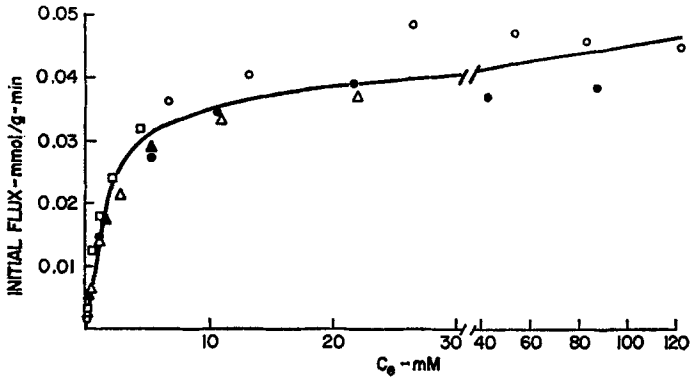


FIGURE 10. Calculated initial influx for $c_i = 0$ from five different experiments, which are indicated by the different symbols. These fluxes are calculated by extrapolating the initial uptake data back to $t = 0$. The curve is calculated from Eq. 3 for $k = 0.056$, $A_o = 23.5$, $B_o = 577$. The curve for $k = 0.047$, $A_o = 24.7$, and $B_o = 600$ is indistinguishable from this one.

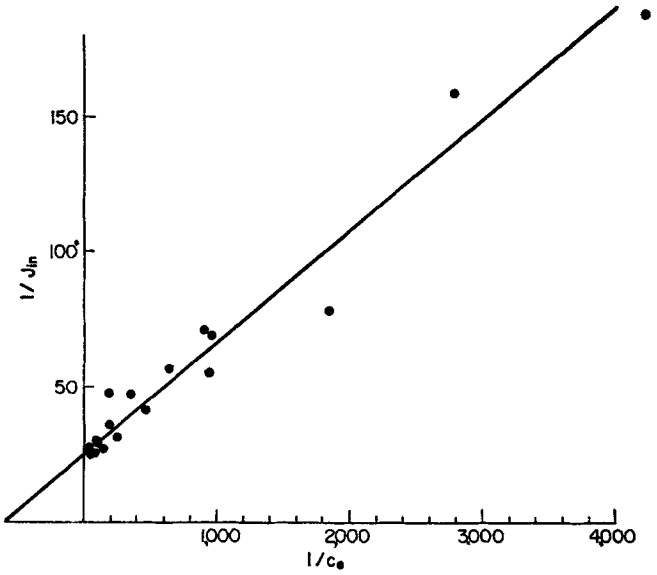


FIGURE 11. Lineweaver-Burk plot of influx data in Fig. 10.

because of the large variability in the data on the plateau in Fig. 10. The inverse plot gave initial estimates of $A_o = 24$, $B_o = 600$, i.e., $J_{M_{in}} = 0.04$ mmol/g-min, $K_{m_{in}} = 1.67 \cdot 10^{-3}$ mmol/ml (1.67 mM).

For the initial flux studies the osmolalities of the AIB solutions were adjusted to 300 mosmol by replacing the calculated amount of the Krebs-Ringer phosphate by water. As a result the extracellular sodium concentrations were lowered. However, the major portion of the initial flux curve is fully defined

for $c_e$ less than 30 mM; in this range the extracellular sodium was decreased by less than 10% from that in the Krebs-Ringer phosphate. Such a decrease in sodium is too small to give a detectable effect on AIB fluxes at these concentrations; the effect would be small even at the higher concentrations of AIB that were used.

According to carrier theory the one-way fluxes depend on both intracellular and extracellular concentrations, so the one-way fluxes may be visualized as surfaces in the three-dimensional spaces with coordinates ($c_i$ , $c_e$ , $J_{in}$) and ($c_i$ , $c_e$ , $J_{ef}$). Fig. 12 combines the data from the steady-state and initial influx studies and shows that these experiments have defined two curves of a surface in the three-space ($c_i$ , $c_e$ , $J_{in}$). The curve for steady-state efflux is the same as the curve for the steady-state data shown in Fig. 12 so it is not presented again. The steady-state fluxes plotted in Fig. 8 are the orthogonal projections of the steady-state curve in three-space on the planes, $c_e - J_{in}$ and $c_i - J_{ef}$.

*Estimation of Parameters*

The parameters in Eqs. 3 and 4 were estimated in stages. In the first stage rough initial estimates were obtained in the following way. The parameters $k$

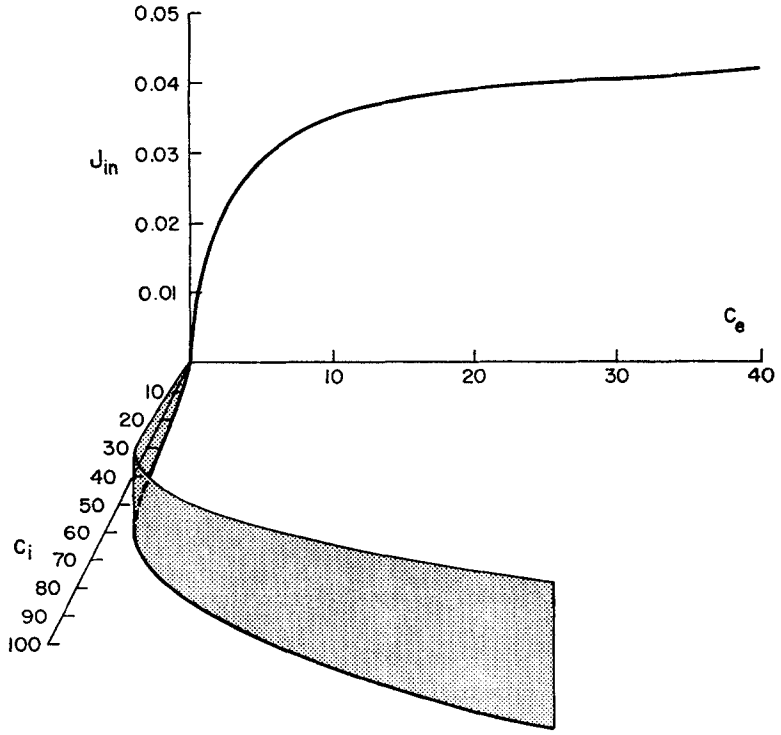


FIGURE 12. Three-dimensional plot showing curves for unidirectional influx for $c_i = 0$ and for the steady state.

$A_o$, and $B_o$ were estimated from the initial flux data, Figs. 10 and 11. $A_1$ was estimated from the steady-state ratio $c_i/c_e$ for $c_e < 1$ mM; on the assumption that the linear terms in Eqs. 3 and 4 are negligible for $c_e$ small; $A_o/A_1 \simeq c_i/c_e$ for $c_e$ small. A crude estimate for $A_2$ was obtained by fitting Eqs. 3 and 4 to some of the data on efflux into 20.5 mM AIB. Finally, $B_1$ and $B_2$ were estimated as was $k$ from the data on steady-state fluxes from relations 11 and 12 which are obtained by rearranging Eqs. 3 and 4.

$$B_1 + B_2 c_e = \frac{c_e}{c_i}\left[\frac{A_o + A_2 c_i}{J_{in} - kc_e}\right] - \frac{c_e}{c_i}\left[B_o + \frac{1}{c_e}\right]. \tag{11}$$

$$B_1 + B_2 c_e = \frac{A_1 + A_2 c_e}{J_{ef} - kc_i} - \frac{c_i}{c_e}\left[B_o + \frac{1}{c_e}\right]. \tag{12}$$

This was done by plotting the right-hand sides of Eqs. 11 and 12 as functions of $c_e$ for a series of values of $k$; the data points so obtained fell approximately on two straight lines. The value of $k$ chosen was that for which the two lines were superimposed, the intercept and slope of this line gave estimates of $B_1$ and $B_2$. This gave the following initial set of parameters: $k = 0.055$ cm³/g-min, $A_o = 24$ cm³/g-min, $B_o = 600$ cm³/mmol, $A_1 = 0.56$ cm³/g-min, $A_2 = 404$ cm⁶/mmol-g-min, $B_1 = 100$ cm³/mmol, $B_2 = 25{,}000$ cm⁶/mmol². This was the starting set for a series of direct fits of Eqs. 3 and 4 by least squares.

The data on initial fluxes were then fitted with use of nonlinear parameter-fitting programs, in two steps. In the first step the parameter space was searched by a sequential univariate search. This gave the values in the first line of Table I. A gradient search from this point in parameter space gave the parameter set of line two in Table I. The mean square in the table is the sum of squares of the residuals around the fitted curve divided by the degrees of freedom in the fitted data. The mean square differs by only 5% for the two sets. Note that $k$ is poorly determined by the initial influx data and this is obvious from the data plotted in Fig. 10. The curve plotted in Fig. 10 is calculated from the first parameter set of Table I. It turned out that on the scale used in Fig. 10 this is indistinguishable from the curve given by parameter set 6, i.e., $k = 0.056$, $A_o = 23.5$, $B_o = 577$. Next, the steady-state data were fitted in all seven parameters simultaneously. This did not give a well-defined minumum in the sum of squares surface. There was a shallow minimum along a curve in the parameter space; for a range of combinations of the seven parameters the mean square varied less than 5% around $0.2 \cdot 10^{-5}$. This implies that the steady-state flux data alone can only determine some combinations of the parameters that have less than seven degrees of freedom. However, the sum of squares increased rapidly as one moved away from the minimum curve suggesting that if one or a few parameters could be fixed by

TABLE I

LEAST SQUARES ESTIMATES OF PARAMETERS

| Fit | Data set | No. of points | $k$ | $A_o$ | $B_o$ | $A_1$ | $B_1$ | $A_2$ | $B_2$ | Residual mean square |
|---|---|---|---|---|---|---|---|---|---|---|
| 1 | I* | 27 | 0.047±0.032‡ | 24.7±3.4 | 600±106 | — | — | — | — | $1.11 \cdot 10^{-5}$ |
| 2 | I | 27 | 0.021±0.032 | 21.4±2.8 | 496±84 | — | — | — | — | $1.06 \cdot 10^{-5}$ |
| 3 | S | 31 | 0.047§ | 24.7§ | 600§ | 0.377±0.05 | 97±11.5 | 589±43 | 35,810±2,400 | $0.23 \cdot 10^{-5}$ |
| 4 | S | 31 | 0.021§ | 21.4§ | 496§ | 0.518±0.079 | 153±21 | 1109±153 | 57,370±8,000 | $0.27 \cdot 10^{-5}$ |
| 5 | I+S | 58 | 0.056±0.015 | 23.5±2.9 | 577±84 | 0.322±0.06 | 77±24 | 440±188 | 28,710±8,900 | $0.227 \cdot 10^{-5}$ |
| 6 | I+S | 58 | 0.092±0.015 | 19.1±2.6 | 476±79 | 0.217±0.041 | 24±3.5 | 124±47 | 13,090‖ | $0.273 \cdot 10^{-5}$ |
| 7 | I+S | 58 | 0.05§ | 15.3±1.5 | 352±41 | 0.201±0.038 | 31±1.4 | 339±34 | 22,700‖ | $0.286 \cdot 10^{-5}$ |

* I, initial influx data; S, steady-state one-way fluxes.

‡ Estimate ± SD of the estimate.

§ The fit was conditioned on this parameter being fixed at the given value.

‖ $B_2$ was constrained by the relation $B_2 = A_2 [B_o/A_o + B_1/A_1 - A_2/A_oA_1]$.

other data, the data on steady-state fluxes might then provide good estimates of the remaining parameters. For this reason a minimization in parameters $A_1$, $B_1$, $A_2$, and $B_2$ was carried out conditional on fixing $k$, $A_o$, and $B_o$ at the two values given by the initial flux data. This gave the two sets of parameters in the third and fourth lines of Table I. The data on initial flux and steady-state fluxes were then fitted simultaneously by weighted least squares. In the weighting the squares of the deviations around the calculated initial flux curve were weighted one-fifth that of the squares of deviations around the steady-state fluxes. In effect the points of each data set were weighted by the inverses of the variances estimated from the mean squares at the minima obtained on each data set alone. This gave the set of parameters in line 5 of Table I. Of the parameters $A_o$, $B_o$, and $A_1$ are determined best by the data, followed by $k$. The three, $B_1$, $A_2$, $B_2$ are not as well determined, with $A_2$ far and away the worst of the set. The continuous curves in Figs. 8 and 10 show that with the above parameter values Eqs. 3 and 4 fit the initial influx data and the steady-state data quite well. The continuous curve in Fig. 9 also shows the distribution ratio predicted for the steady state by parameter set 5 in Table I. This was obtained by equating relations 3 and 4 and solving for $c_i/c_e$ as a function of $c_e$. Again, the fit is quite good except for values of $c_e$ below 0.3 mM. This might be expected for two reasons. For one, the error in determining $c_i/c_e$ increases as $c_e$ becomes smaller as attested by the increasing scatter in the $c_i/c_e$ values for low $c_e$. More importantly, the parameter sets in Table I were obtained by fitting the data on fluxes and since the fluxes at very small $c_e$ are quite small they carry less weight in the least squares estimation procedure. The parameter set on line 3 of Table I gave a somewhat better fit to the data on steady-state distribution ratio for $c_e < 0.3$ mM but was no better at higher $c_e$.

The parameters of fit 5 in Table I satisfy the constraint given by Eq. 8 within the errors of the estimates of the parameters. However, to see how constraint 8 would affect the fit, line 6 gives the results of a least square fit in which $B_2$ was constrained by relation 8. From previous work in this laboratory (18, 44), the estimate of 0.092 for $k$ seemed high. A good estimate from all of the previous work done here is $k = 0.05$ so the constrained fit was redone with $k$ set at 0.05, giving parameter set 7 of Table I. The general pattern of the results remains the same as for the unconstrained fit although the fit to the data is not quite as good as for parameter set 5. In particular set 6 does not give as good a fit to the influx data as do sets 5 and 7.

*Steady-State Studies at Other* $[Na^+]_e$ *and* $[K^+]_e$

When these studies were started it was my intention to examine the effect of a series of different extracellular and intracellular sodium and potassium concentrations on one-way fluxes, to estimate the parameters of Eqs. 3 and 4 and

thus determine the dependence of these parameters on the ion concentrations. As may be seen from the large amount of data needed to obtain the estimates given in Table I, this program turned out to be impractical. However, a few studies on one-way fluxes in the steady state were completed at different $[Na^+]_e$ and $[K^+]_e$. Besides the experiments already reported for $[K^+]_e$ = 8.8 mM, a few were also obtained for $[K^+]_e$ = 3 and 22–25 mM. The former were done for $[Na^+]_e$ = 5 and 150 meq/liter, the latter for $[Na^+]_e$ = 5, 10, 20, 40, 123 meq/liter. Table II gives the intracellular and extracellular sodium and potassium concentrations in these experiments. For each $[Na^+]_e$ and $[K^+]_e$ combination, seven experiments were run over a range of extracellular concentrations of AIB of 0.05–25 mM. As in the other experiments, it was found that intracellular potassium generally fell in going from low $c_e$ to high $c_e$. The highest and lowest values in each set of seven experiments are given in Table II. If anything, this phenomenon was more obvious in this set of experiments.

TABLE II

EXTRACELLULAR AND INTRACELLULAR CONCENTRATIONS OF SODIUM AND POTASSIUM IN STEADY-STATE EXPERIMENTS

| $[Na^+]_e$ | $[K^+]_e$ | $[Na^+]_i$ | $[K^+]_i$ |
|---|---|---|---|
| 123.6 | 21.9 | 14.0 | 179-116 |
| 39.5 | 24.3 | 9.3 | 184-96 |
| 20.2 | 24.8 | 8.3 | 173-100 |
| 9.5 | 25.3 | 7.8 | 172-110 |
| 5.1 | 24.4 | 5.6 | 178-130 |
| 148 | 2.8 | 25.2 | 156-109 |
| 4.7 | 3.0 | 4.8 | 145-94 |

Fig. 13 shows the one-way influx of AIB in the steady state as a function of extracellular concentrations for $[Na^+]_e$ = 5, 10, 20, 40, and 123 meq/liter for $[K^+]_e$ = 22–25 meq/liter. The points at 5 and 10 meq/liter $[Na^+]_e$ overlapped so much that only one curve was drawn through them. The points at 20 meq/liter $[Na^+]_e$ came quite close to those for 40 so a separate curve is not drawn through them either. From previous results (18) one would expect that the curves for influx would increase progressively with increase in $[Na^+]_e$ and this is in general what was found although the data for $[Na^+]_e$ = 5 and 10 meq/liter are not clearly separated and the points for $[Na^+]_e$ = 20 meq/liter come close to the curve for $[Na^+]_e$ = 40 meq/liter. It seems likely that there is actually a progressive increase in the influx curves as $[Na^+]_e$ increases but that the differences between the fluxes for 5 and 10 meq/liter $[Na^+]_e$ and the differences between those for 20 and 40 meq/liter are too small to be demonstrated with the small number of points obtained and the inherent fluctuation in the steady-state experiments. Fig. 14 shows the one way efflux as function of the intracellular concentration for these same experiments. The data for the

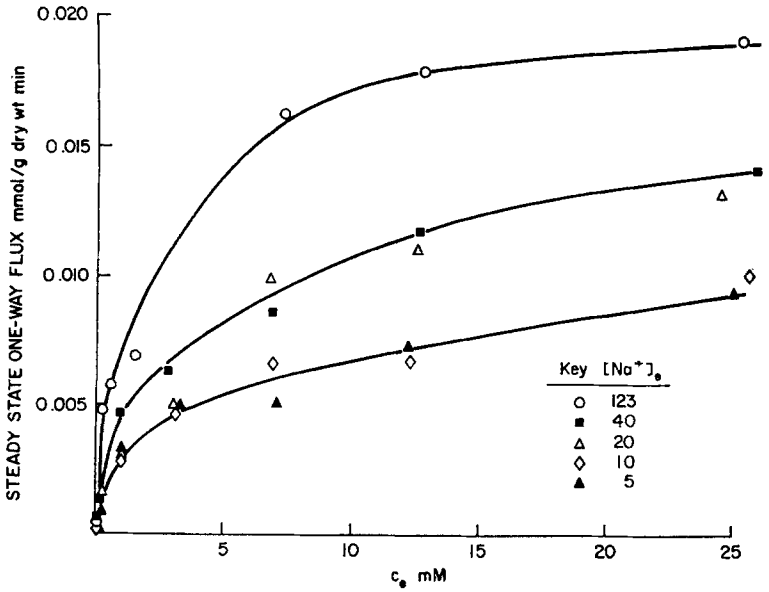


FIGURE 13. One-way influxes in the steady state for $[K^+]_e$ = 22–25 mM for different extracellular concentrations of sodium.

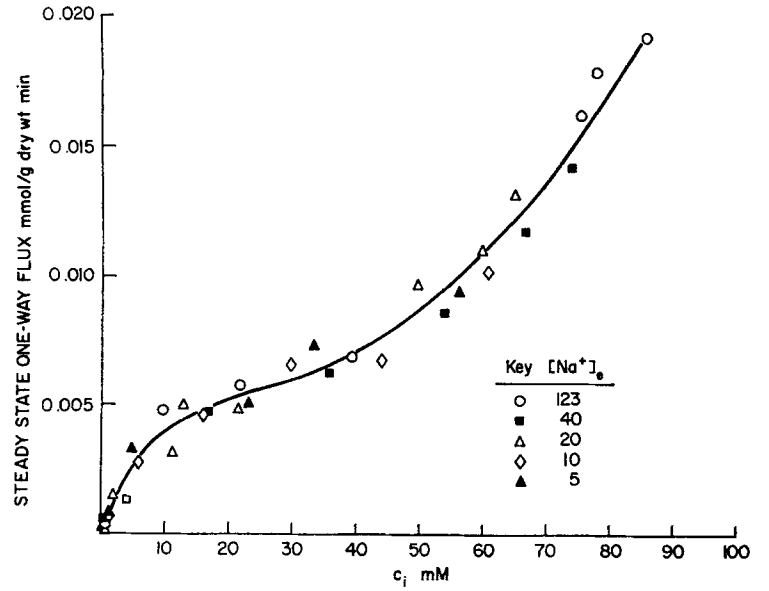


FIGURE 14. One-way effluxes as function of $c_i$ for the experiments shown in Fig. 13.

experiments run at different $[Na^+]_e$ appear to fall on the same curve but this appearance is deceptive. Since the efflux may in general be a function of $c_e$, $c_i$, $[Na^+]_e$, and $[Na^+]_i$, (see Eqs. 3, 4, and the Appendix) it should be emphasized that the steady-state efflux data in Fig. 14 for the different $[Na^+]_e$

represent projections on the $c_i$-$J_{ef}$ plane of different curves in the three-space ($c_i$, $c_e$, $J_{ef}$); all of these projections are plotted together in Fig. 14. For example, consider the three points, for $[Na^+]_e$ = 123, 20, and 5 that fall close together at $c_i \simeq 22$ mM in Fig. 14, for these, $c_e$ = 0.69, 3.1, and 7.1, respectively. Fig. 15 illustrates this for the data for $[Na^+]_e$ = 5 and 123, the other points are not included in this graph because their inclusion cluttered up the graph and confused the picture. The point I would emphasize is that from an examination of Fig. 14, one may not conclude that the efflux of AIB is independent of the *trans* sodium concentration $[Na^+]_e$, because the other variables that affect efflux are not constant; for fixed $c_i$, $c_e$ increases as $[Na^+]_e$

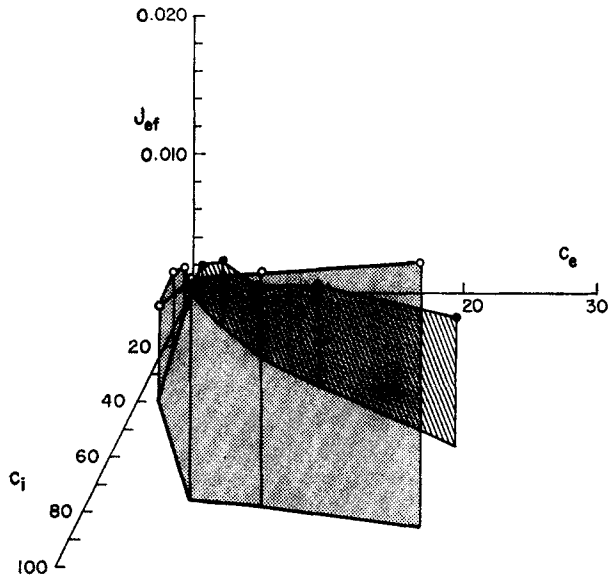


FIGURE 15. Three-dimensional plot of the one-way fluxes for $[Na^+]_e$ = 5 and 123 meq/liter from Figs. 13 and 14.

decreases and the effects of these two changes are in opposition. It happens that the projections on the $c_i$-$J_{ef}$ plane of the curves for different $[Na^+]_e$ fall close together. This argument is fortified by the data obtained at $[K^+]_e$ = 3 mM which are shown in Figs. 16 and 17. Now there is a clear difference between the curves for $[Na^+]_e$ = 5 and 150 for one-way influx and efflux. Nonetheless, the same warning should be made as has been given above. Figs. such as 16 and 17 may be misinterpreted unless one remembers that $J_{in}$ and $J_{ef}$ are functions of $c_e$, $c_i$, $[Na]_e$, and $[Na]_i$, and perhaps other variables, and the variables not shown in Figs. 16 and 17 are not constant along any one curve.

## DISCUSSION

It is clear from the data that the one-way fluxes show a *trans* effect in the concentrations of AIB. Thus, dependence of one-way influx on extracellular con-

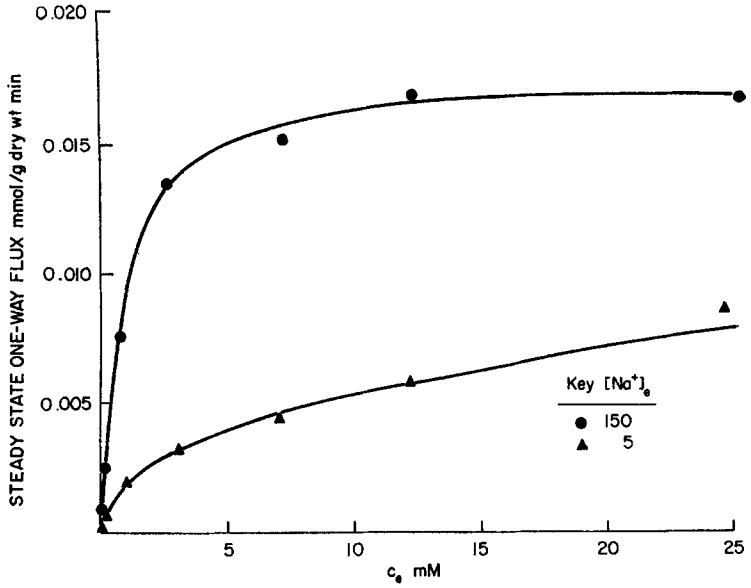


FIGURE 16. One-way influxes as function of $c_e$ for the steady state at $[K^+]_e = 3$ mM.

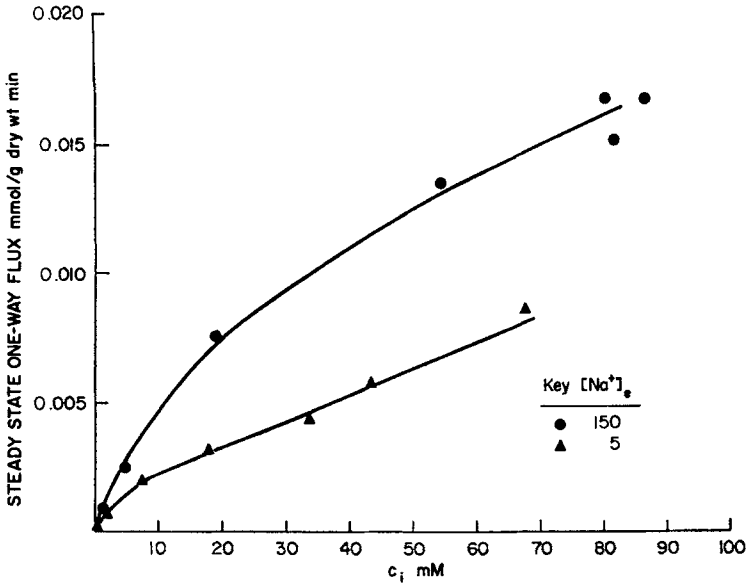


FIGURE 17. One-way effluxes as function of $c_i$ for the experiments shown in Fig. 16.

centration is different for $c_i = 0$, Fig. 10, from that in the steady-state for which $c_i$ increases as $c_e$ does, Fig. 8. For given $c_e$ the steady-state influx is less than when $c_i = 0$. This difference could not be present if the one-way influx depended only on the extracellular concentrations. Thus, we have direct evidence for a *trans* inhibition in the *one-way* influx. I have also obtained curves

of efflux from cells loaded with AIB and although such efflux studies have always been poor because of a large variation in replicates, I have never obtained curves that even slightly resemble the curve for efflux shown in Fig. 8, suggesting that there are *trans* effects in one-way effluxes as well as in the influxes.

Having obtained evidence for *trans* effects in the one-way fluxes, the next problem was to see whether the two-state carrier model shown in Fig. 1, and which is used so commonly to describe the kinetics of active transport, is consistent with the data obtained in these studies. To this end the parameters in Eqs. 3 and 4 were estimated from the steady-state one-way fluxes and the initial influx at $c_i = 0$. The values of the parameters obtained are given in Table I. Recall that all of the data in these studies are from 32°C and for $[Na^+]_e = 143$ meq/liter and $[K^+]_e = 8.8$ meq/liter. The value of $k$ obtained is consistent with the values obtained in previous studies on net influxes carried out at 37°C (18, 44). Eqs. 3 and 4, with the parameter values in line 5 of Table I, give the curves plotted in Figs. 8, 9, and 10, which fit the data on steady-state one-way fluxes, steady-state distribution ratios, and initial influx at $c_i = 0$ quite well. Table III gives the one-way fluxes predicted by parameter set 5 for a set of values of $c_e$ and $c_i$ and shows that for these parameters

TABLE III

ONE-WAY FLUXES PREDICTED BY EQUATIONS OF TWO-STATE CARRIER MODEL*

| $c_e$ | $c_i$ | $J_{in}$ | $J_{ef}$ |
|---|---|---|---|
| *mM* | *mM* | *mmol/g-min* | *mmol/g-min* |
| 0 | 0 | — | — |
| | 1 | — | 0.00036 |
| | 10 | — | 0.00238 |
| | 40 | — | 0.00540 |
| 1 | 0 | 0.0150 | — |
| | 1 | 0.0143 | 0.00051 |
| | 10 | 0.0106 | 0.00343 |
| | 40 | 0.0071 | 0.00749 |
| 10 | 0 | 0.0353 | — |
| | 1 | 0.0341 | 0.00072 |
| | 10 | 0.0274 | 0.00510 |
| | 40 | 0.0198 | 0.01110 |
| 40 | 0 | 0.0413 | — |
| | 1 | 0.0401 | 0.00076 |
| | 10 | 0.0330 | 0.00549 |
| | 40 | 0.0247 | 0.01205 |

* For parameter set 5 of Table I.

the two-state carrier model predicts a *trans* inhibition of influx and a *trans* stimulation of efflux. The *trans* inhibition of influx has been demonstrated for initial 1-min influxes (18, 44) and in the data reported here for one-way influxes. I also have evidence for *trans* stimulation of efflux. For cells loaded to intracellular levels of 14.9–26.7 mM AIB the efflux into KRP with $c_e < 0.1$ mM was 0.0026 ± 0.0007 (SE) in five experiments whereas the one-way efflux in the steady-state studies for $c_i$ in the same range of values was 0.004–0.005. Given the estimated parameters $A_o \cdots B_2$, is it possible to determine the kinetic parameters of the carrier model? It would appear not for as is shown in the Appendix, there are eight independent basic parameters in the carrier model but only five independent parameters of the set $A_o \cdots B_2$.

It is important to emphasize the significance of the fact that the standard carrier model with the same passive permeability for one-way influx and efflux fits all of the data obtained. With more limited data it might be possible to interpret the data in terms of Eqs. 1 and 2 but with *different* passive permeabilities for influx and efflux. For example, if the data in Fig. 8 were restricted to concentrations below 100 mM one could fit influx and efflux with Eqs. 1 and 2, respectively, but the long approximately linear portion of the efflux curve between $c_i = 10$ and $c_i = 100$ mM would give an apparent $k$ for efflux much larger than the $k$ obtained for influx. The data on initial influx in Fig. 10 could then be fitted by Eq. 1 but the $J_{M_{in}}$ and $K_{m_{in}}$ obtained would differ from those obtained for the steady-state influx. It is significant that all of the data are fitted by one model, the common carrier model, that uses the same passive permeability for influx and efflux and which then predicts *trans* inhibition of influx and *trans* stimulation of efflux.

In summary the findings of this study are as follows: (*a*) *Trans* effects of AIB on the *one-way fluxes* of AIB have been demonstrated unequivocally. (*b*) The two-state carrier model gives good fits to both initial fluxes ($c_i = 0$) and to steady-state one-way fluxes. (*c*) With use of the parameters obtained by fitting the initial fluxes and the steady-state one-way fluxes the two-state carrier model predicts a *trans* inhibition of influx and a *trans* stimulation of efflux. Both of these effects have been demonstrated experimentally, the former more securely than the latter. None of this is proof of the validity of the common carrier model but it does demonstrate its consistency with the experimental results on AIB.

Finally, I think it is important to seek other experiments for estimating the parameters of Eqs. 3 and 4 to see if the values obtained are consistent for a wider range of flux measurements. In my experience the one-way efflux experiments are not good for this for reasons that have already been given. However, net fluxes can be obtained for a wide range of intracellular and extracellular concentrations for cells treated the same way as were those used in the present studies of initial influxes and steady-state fluxes. Such studies would

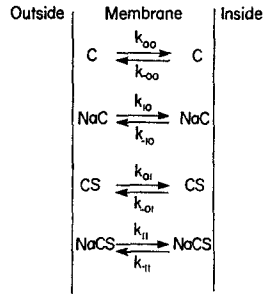


FIGURE 18. Two-state carrier model with cotransport of sodium.

give another set of estimates of $k$, $A_o$, $B_o$, $A_1$, $B_1$, and $B_2$ but $A_2$ cannot be estimated from net fluxes. These studies are under way now.

## APPENDIX

Fig. 18 shows the different carrier complexes that can be formed in an ion cotransport model in which only sodium combines with carrier and substrate to form a 1:1:1 complex. The different transition rate constants are shown in the figure. The dissociation constants are assumed to be the same at the two sides of the membrane and are given by relations 1 *a*–3 *a*.

$$K_{10} = \frac{[Na][C]}{[NaC]}. \tag{1 a}$$

$$K_{01} = \frac{[C][S]}{[CS]}. \tag{2 a}$$

$$K_{11} = \frac{[Na][C][S]}{[NaCS]}. \tag{3 a}$$

Eight particular combinations of the transition rate constants and dissociation constants appear in the equations corresponding to Eqs. 3 and 4. These are defined by equations 4 *a*–7 *a*.

$$e_o = k_{oo} + \frac{k_{10}[Na]_e}{K_{10}}, \qquad e_1 = \frac{k_{01}}{K_{01}} + \frac{k_{11}[Na]_e}{K_{11}}. \tag{4 a}$$

$$f_o = k_{-oo} + \frac{k_{-10}[Na]_i}{K_{10}}, \qquad f_1 = \frac{k_{-01}}{K_{01}} + \frac{k_{-11}[Na]_i}{K_{11}}. \tag{5 a}$$

$$g_o = 1 + \frac{[Na]_e}{K_{10}}, \qquad g_1 = \frac{1}{K_{01}} + \frac{[Na]_e}{K_{11}}. \tag{6 a}$$

$$h_o = 1 + \frac{[Na]_i}{K_{10}}, \qquad h_1 = \frac{1}{K_{01}} + \frac{[Na]_i}{K_{11}}. \tag{7 a}$$

Using these intermediate parameters, one can show (35) that parameters $A_o \cdots B_2$ are given by relations 8 *a*–10 *a*.

$$A_o = \frac{C_o e_1 f_o}{e_o h_o + f_o g_o}, \qquad B_o = \frac{e_1 h_o + f_o g_1}{e_o h_o + f_o g_o}. \tag{8 a}$$

$$A_1 = \frac{C_o e_o f_1}{e_o h_o + f_o g_o}, \qquad B_1 = \frac{e_o h_1 + f_1 g_o}{e_o h_o + f_o g_o}. \tag{9 a}$$

$$A_2 = \frac{C_o e_1 f_1}{e_o h_o + f_o g_o}, \qquad B_2 = \frac{e_1 h_1 + f_1 g_1}{e_o h_o + f_o g_o}. \tag{10 a}$$

The constraint given by Eq. 8 still holds. Of the eight transition rate constants only four are independent (35). Thus, there are four independent transition rate constants, three dissociation constants, plus the concentration of carrier, a total of eight basic constants that appear in rather involved combinations in five independent parameters, $A_o$, $A_1$, $A_2$, $B_o$, $B_1$, that are estimated from the data.

I thank Mr. Eugene Daniels for his help in programming the nonlinear least squares computations used for estimation of parameters.

This work was supported in part by grant CA06734 from the National Cancer Institute, DHEW.

*Received for publication 14 May 1974.*

## REFERENCES

1. HEINZ, E. 1954. Kinetic studies on the "Influx" of Glycine-1-$C^{14}$ into the Ehrlich mouse ascites carcinoma cell. *J. Biol. Chem.* **211**:781–790.
2. HEINZ, E., and H. A. MARIANI. 1957. Concentration work and energy dissipation in active transport of glycine into carcinoma cells. *J. Biol. Chem.* **228**:97–111.
3. TENNENHOUSE, A., and J. H. QUASTEL. 1960. Amino acid accumulation in Ehrlich ascites carcinoma cells. *Can. J. Biochem. Physiol.* **38**:1311–1326.
4. NEAME, K. D., and T. G. RICHARDS. 1972. Elementary Kinetics of Membrane Carrier Transport. John Wiley & Sons, Inc., N.Y.
5. HEINZ, E., and P. M. WALSH. 1958. Exchange diffusion, transport and intracellular level of amino acids in Ehrlich carcinoma cells. *J. Biol. Chem.* **233**:1488–1493.
6. JOHNSTONE, R. M., and P. G. SCHOLEFIELD. 1961. Factors controlling the uptake and retention of methionine and ethionine by Ehrlich ascites carcinoma cells. *J. Biol. Chem.* **236**:1419–1424.
7. JACQUEZ, J. A. 1961. Transport and exchange diffusion of L-tryptophan in Ehrlich cells. *Am. J. Physiol.* **200**:1063–1068.
8. JACQUEZ, J. A. 1963. Carrier-amino acid stoichiometry in amino acid transport in Ehrlich ascites cells. *Biochim. Biophys. Acta.* **71**:15–33.
9. OXENDER, D., and H. N. CHRISTENSEN. 1963. Distinct mediating systems for the transport of neutral amino acids by the Ehrlich cell. *J. Biol. Chem.* **238**:3686–3699.
10. GILLESPIE, E. 1967. Homo- and hetero-exchange diffusion of amino acids in Ehrlich ascites carcinoma cells. *Biochim. Biophys. Acta.* **135**:1016–1029.
11. SCHWARTZMAN, L., A. BLAIR, and S. SEGAL. 1967. Exchange diffusion of dibasic amino acids in rat-kidney cortex slices. *Biochim. Biophys. Acta.* **135**:120–126.
12. CLAYMAN, S., and P. G. SCHOLEFIELD. 1969. The uptake of amino acids by mouse pancreas in vitro. IV. The role of exchange diffusion. *Biochim. Biophys. Acta.* **173**:277–289.

13. JOHNSTONE, R. M., and P. G. SCHOLEFIELD. 1965. Amino acid transport in tumor cells. *Adv. Cancer Res.* **9**:143–226.
14. PAINE, C. M., and E. HEINZ. 1960. The structural specificity of the glycine transport system of Ehrlich carcinoma cells. *J. Biol. Chem.* **235**:1080–1085.
15. OXENDER, D. L., and H. N. CHRISTENSEN. 1963. Evidence for two types of mediation of neutral amino acid transport in Ehrlich cells. *Nature (Lond.)*. **197**:765–767.
16. RING, K., and E. HEINZ. 1966. Active amino acid transport in Streptomyces hydrogenans. I. Kinetics of uptake of $\alpha$-aminoisobutyric acid. *Biochem. Z.* **344**:446–461.
17. BELKHODE, and P. G. SCHOLEFIELD. 1969. Interactions between amino acids during transport and exchange diffusion in Novikoff and Ehrlich ascites tumor cells. *Biochim. Biophys. Acta.* **173**:290–301.
18. JACQUEZ, J. A. 1973. Sodium dependence of maximum flux, $J_M$, and $K_m$ of amino acid transport in Ehrlich ascites cells. *Biochim. Biophys. Acta.* **318**:411–425.
19. WIDDAS, W. F. 1952. Inability of diffusion to account for placental glucose transfer in the sheep and consideration of the kinetics of a possible carrier transfer. *J. Physiol. (Lond.)*. **118**:23–39.
20. ROSENBERG, T., and W. WILBRANDT. 1955. The kinetics of membrane transports involving chemical reactions. *Exp. Cell Res.* **9**:49–67.
21. JACQUEZ, J. A. 1961. The kinetics of carrier-mediated active transport of amino acids. *Proc. Natl. Acad. Sci. U.S.A.* **47**:153–163.
22. JACQUEZ, J. A. 1964. The kinetics of carrier-mediated transport: Stationary-state approximations. *Biochim. Biophys. Acta.* **79**:318–328.
23. REGEN, D. M., and H. E. MORGAN. 1964. Studies of the glucose-transport system in the rabbit erythrocyte. *Biochim. Biophys. Acta.* **79**:151–166.
24. WONG, J. T. 1965. The possible role of polyvalent carriers in cellular transports. *Biochim. Biophys. Acta.* **94**:102–113.
25. BRITTEN, H. G. 1965. Fluxes in passive, monovalent and polyvalent carrier systems. *J. Theor. Biol.* **10**:28–52.
26. HELMREICH, E., and D. M. KIPNIS. 1962. Amino acid transport in lymph node cells. *J. Biol. Chem.* **237**:2582–2589.
27. SCHULTZ, S. G., and P. F. CURRAN. 1970. Coupled transport of sodium and organic solutes. *Physiol. Rev.* **50**:637–718.
28. HEINZ, E., editor 1972. Na-Linked Transport of Organic Solutes. Springer-Verlag GmbH, Berlin.
29. INUI, Y., and H. N. CHRISTENSEN. 1966. Discrimination of single transport systems. *J. Gen. Physiol.* **50**:203–224.
30. CURRAN, P. F., S. G. SCHULTZ, R. A. CHEZ, and R. E. FUISZ. 1967. Kinetic relations of the Na-amino acid interaction at the mucosal border of intestine. *J. Gen. Physiol.* **50**:1261–1286.
31. EDDY, A. A., M. F. MULCAHY, and P. J. THOMSON. 1967. The effects of sodium ions and potassium ions on glycine uptake by mouse ascites-tumor cells in the presence and absence of selected metabolic inhibitors. *Biochem. J.* **103**:863–876.
32. EDDY, A. A. 1968. A net gain of sodium ions and a net loss of potassium ions accompanying the uptake of glycine by mouse ascites-tumor cells in the presence of sodium cyanide. *Biochem. J.* **108**:195–206.
33. MORVILLE, M., M. REID, and A. A. EDDY. 1973. Amino acid absorption by mouse ascites-tumor cells depleted of both endogenous amino acids and adenosine triphosphate. *Biochem. J.* **134**:11–26.
34. HEINZ, E., P. GECK, and W. WILBRANDT. 1972. Coupling in secondary active transport. Activation of transport by co-transport and/or counter-transport with the fluxes of other solutes. *Biochim. Biophys. Acta.* **255**:442–461.
35. JACQUEZ, J. A. 1972. Models of ion and substrate cotransport and the effect of the membrane potential. *Math. Biosci.* **13**:71–93.
36. VIDAVER, G. A. 1964. Transport of glycine by pigeon red cells. *Biochemistry.* **3**:662–667.

37. VIDAVER, G. A., and S. L. SHEPHARD. 1968. Transport of glycine by hemolyzed and restored pigeon red blood cells. *J. Biol. Chem.* **243**:6140–6150.
38. RIGGS, T. R. L., M. WALKER, and H. N. CHRISTENSEN. 1958. Potassium migration and amino acid transport. *J. Biol. Chem.* **233**:1479.
39. HEINZ, E. 1957. The exchangeability of glycine accumulated by carcinoma cells. *J. Biol. Chem.* **225**:305–315.
40. KIPNIS, D. M., E. REISS, and E. HELMREICH. 1961. Functional heterogeneity of the intracellular amino acid pool in mammalian cells. *Biochim. Biophys. Acta.* **51**:519–524.
41. JACQUEZ, J. A. 1972. Compartmental Analysis in Biology and Medicine. Elsevier Scientific Publishing Co., Amsterdam.
42. CHRISTENSEN, H. N., C. DECESPEDES, M. E. HANDLOGTEN, and G. RONQUIST. 1974. Modified transport substrates as probes for intramembrane gradients. *Ann. N.Y. Acad. Sci.* **227**:355.
43. HEMPLING, H. G. 1958. Potassium and sodium movements in the Ehrlich mouse ascites tumor cell. *J. Gen. Physiol.* **41**:565–583.
44. JACQUEZ, J. A., J. H. SHERMAN, and J. TERRIS. 1970. Temperature dependence of amino acid transport in Ehrlich ascites cells; with results which bear on the A-L distinction. *Biochim. Biophys. Acta.* **203**:150.